FOI-R—1378--SE
December 2004
ISSN 1650-1942
Technical Report

Torgny Carlsson, Martin Norrefeldt, Mattias Elfsberg, Sara Wallin

High Speed Combustion – Activities during 2004

Weapons and Protection
SE-147 25 TUMBA

SWEDISH DEFENCE RESEARCH AGENCY
Weapons and Protection
SE-147 25 Tumba

FOI-R--1378--SE
December
ISSN 1650-1942
Technical Report

Torgny Carlsson, Martin Norrefeldt, Mattias Elfsberg, Sara Wallin

High Speed Combustion – Activities during 2004

Issuing organization	Report number, ISRN	Report type
Swedish Defence Research Agency Weapons & Protection SE-172 90 Stockholm	FOI-R—1378—SE	Technical Report
	Research area code 5	
	Month year December 2004	**Project no.** E2006
	Customers code Contracted Research	
	Sub area code 51	

Author/s (editor/s)	Project manager
Torgny Carlsson Martin Norrefeldt Mattias Elfsberg Sara Wallin	Bengt Eiderfors
	Approved by Jon Tegner
	Scientifically and technically responsible Torgny Carlsson

Report title

High Speed Combustion – Activities during 2004

Abstract (not more than 200 words)

An account is given for the work that has been done to study high speed combustion during 2004 in the FOI-project, Framdrivning (Propulsion). The high speed combustion work was initiated with the aim to develop FOI:s competence in new experimental techniques for combustion diagnostics. The experimental methods used are LIF - Laser Induced Fluorescence, shadow, schlieren and interferometrical methods (primarily holography), the latter in cooperation with LTU–Luleå Technical University. This report describes the changes and the improvements which have been done to the experimental technique used for PLIF (Planar Laser Induced Fluorescence). It also describes the development of evaluation methods to combine schlieren and interferometry in order to benefit from the advantages of each of them. The experiments were done in the high speed combustion rig which has been built in this project, where the propagation of a high speed turbulent flame jet of an air/hydrogen gas mixture was studied. Descriptions are given of the experimental results and the evaluation of the results.

Keywords

propulsion, combustion, experimental methods, laser induced fluorescence, shadow and schlieren technique, interferometry, holography

Further bibliographic information	Language English
ISSN 1650-1942	**Pages** 33 p.
	Price acc. to pricelist
	Security classification

Utgivare Totalförsvarets Forskningsinstitut – FOI Vapen & skydd 172 90 Stockholm	**Rapportnummer, ISRN** FOI-R--1378—SE	**Klassificering** Teknisk rapport
	Forskningsområde 5	
	Månad, år December 2004	**Projektnummer** E2006
	Verksamhetsgren Uppdragsfinansierad verksamhet	
	Delområde 51	

Författare/redactor Torgny Carlsson Martin Norrefeldt Mattias Elfsberg Sara Wallin	**Projektledare** Bengt Eiderfors
	Godkänd av Jon Tegner
	Tekniskt och/eller vetenskapligt ansvarig Torgny Carlsson

Rapportens titel (i översättning)

Höghastighetsförbränning – Verksamhet under 2004

Sammanfattning (högst 200 ord)

En redogörelse ges av det arbete som bedrivits under 2004 i projektet Framdrivning för diagnostisering av HHF – höghastighetsförbränning. Verksamhetens syfte är att utveckla FOIs förmåga att utnyttja nya experimentella tekniker för förbränningsstudier. De mätmetoder som används är LIF – Laserinducerad fluorescens, slir-, skugg- och interferometrisk teknik (framförallt holografi), det senare i samarbete med LTU–Luleå tekniska universitet. I denna rapport beskrivs dels förändringar och förbättringar av den experimentella teknik som används för PLIF (Planar Laser Induced Fluorescence), dels utvecklingen av utvärderingsmetoder för att kombinera interferometri och slirmätningar i syfte att utnyttja vardera metodens fördelar och på så sätt förbättra mätningarnas noggrannhet och tillförlitlighet. Experimenten har utförts i den i projektet uppbyggda förbränningsriggen, där utbredning av en jetstråle som uppkommer pga. förbränning av luft/vätgas-blandning i en kavitet med ett litet utblåsningshål har studerats. En redovisning ges av de experimentella resultaten och utvärderingarna av dessa.

Nyckelord

framdrivning, förbränning, experimentella metoder, laserinducerad fluorescens, skugg- och slirteknik, interferometri

Övriga bibliografiska uppgifter	**Språk** Engelska
ISSN 1650-1942	**Antal sidor:** 33 s.
Distribution enligt missiv	**Pris: Enligt prislista** **Sekretess**

Contents

1. Sammanfattning

För att förstå och förbättra framdrivningssystem krävs experimentella studier av olika förbränningsprocesser. Även om datorstödd modellering blir allt mer kraftfull, är experiment en förutsättning för att kunna validera och utveckla modellerna. Under åren har det utvecklats ett otal olika typer av sensorer och experimentella tekniker för detta syfte [1]. Vad som eftersträvas är mätmetoder som har förmåga att ta upp två- och tredimensionell information om bl.a. koncentration, densitet, tryck, temperatur och hastighet utan att störa de studerade processerna. De tekniker som är mest lämpade för detta är optiska, beröringsfria mätmetoder.

I denna rapport beskrivs den verksamhet som bedrivits under 2004 i projektet Framdrivning för diagnostisering av HHF – höghastighetsförbränning. Denna verksamhet initierades med syftet att utveckla FOIs förmåga att utnyttja nya experimentella tekniker för förbränningsstudier. Arbetet har koncentrerats på LIF – laserinducerad fluorescens, interferometri, skugg- och sliravbildning. De interferometriska mätningarna görs i samarbete med avd. Experimentell mekanik vid LTU – Luleå tekniska universitet. Verksamheten har tidigare redovisats i rapporter [2-7] och tidskriftsartiklar [8,9], för mer detaljer hänvisas till dessa. Här beskrivs det fortsatta arbetet med LIF, sliravbildning och interferometri. Experimenten har utförts i den i projektet uppbyggda förbränningsriggen, där utbredning av en jetstråle som uppkommer pga. förbränning av luft/vätgas-blandning i en kavitet med ett litet utblåsningshål har studerats.

PLIF – “Planar Laser Induced Fluorescence”, är en variant av LIF och en av de vanligast använda metoderna för förbränningsstudier. PLIF är en känslig metod som kan användas för tvådimensionell avbildning av ett tunt snitt av förbränningsområdet. Det som framförallt kan studeras är koncentrationsfördelningen av förbränningsprodukter (här OH), men även temperaturfördelningar och, för mycket snabba förlopp, hastighetsfördelningar. Arbetet har främst inriktats mot förbättring av utrustning och utvärderingsmetoder. Lasern har bytts ut och triggsystemet har förändrats, allt med lyckade resultat. Dock, kvarstår svårigheter att detektera OH från luft/vätgas förbränningen i riggen. Det kan finnas flera orsaker till detta, bl.a. att ljusets intensitet och andelen OH inte är tillräckligt stora för att kunna detekteras av den kamera som används. Detta skall undersökas vidare bl.a. genom att använda andra gasblandningar och genom att reducera trycket för att undvika s.k. ”quenching” (utsläckning).

Sliravbildning och interferometri är känsliga för brytningsindexförändringar, vilket i sin tur är proportionella mot densitetsförändringar. Utvärderingsalgoritmer har utvecklats för att kombinera dessa metoder i syfte att utnyttja vardera metodens fördelar och på så sätt förbättra mätningarnas noggrannhet och tillförlitlighet [9]. Abeltransformering användes för att erhålla den tredimensionella densitetsfördelningen. De försök som genomfördes i HHF-riggen gav mycket god kvalitativ överensstämmelse mellan de olika metoderna och, genom användning av den nya utvärderingsmetodiken, också goda kvantitativa värden.

2. Introduction

Experimental studies of combustion processes are necessary to understand how they work, to enable improvements of propulsion systems and as an aid to computer modelling. Over the years, almost innumerable sensors and experimental techniques have been developed for this purpose [1]. Since it is almost impossible to use a sensor that needs to be in some kind of contact with a reacting flow without disturbing it, non-intrusive (mainly optical) techniques presents an attractive alternative.

The following report describes the work that has been done to study high speed combustion during 2004 in the FOI-project, Framdrivning (Propulsion). The high speed combustion work was initiated with the aim to develop FOI:s competence in new experimental techniques for combustion diagnostics. The project work has mainly been focused on LIF – Laser Induced Fluorescence, interferometry, shadow and schlieren imaging. This has been been accounted for in previous reports [2-7] and journal articles [8,9], for more details about the methods used, we refer to these.

In chapter 2, a description is given of the combustion rig which has been built in this project, and in which most of the project work has been carried out. The experiment which is referred to in this report is described, i.e. the propagation of a high speed turbulent flame jet of an air/hydrogen gas mixture.

Chapter 3 reports the work done with PLIF (Planar Laser Induced Fluorescence), which is a variety of LIF. It is one of the most widely used methods for combustion analysis. PLIF is very sensitive and can be used for two-dimensional imaging of a thin slice of the combustion zone. It can be used to study concentrations of combustion gases and products and for temperature measurement. In this project we have chosen to use OH (hydroxide) as probe. For more information about LIF and combustion diagnostics, see [7].

Chapter 4 describes the development of interferometry and schlieren techniques. These methods are sensitive to changes of index of refraction which is closely related to density changes. During the last year, these methods have been further improved. The air/hydrogen jet has been studied with the schlieren and the pulsed TV holography method. These methods have been compared and combined to benefit from the advantages of each of them [9]. Abel inversion has been used to achieve three-dimensional information regarding refractive index distributions. The results obtained from the different techniques show remarkable similarities concerning both qualitative and quantitative aspects.

The report ends with conclusions and discussions about future work. Materials of highly technical content are collected in five appendixes.

3. The high-speed combustion rig

3.1 The rig design

The high-speed combustion rig at FOI Grindsjön (see figure 1 and 2) is designed for development and testing of different optical techniques for experimental combustion studies. It is made of stainless steel with a quadratic cross section (60×60 mm^2). It is modularly designed, where each module is 210 mm long. All modules are prepared with inputs, which can e.g. be used for gas inlets and outlets, spark plugs to ignite combustion, and to attach pressure gauges and other sensors. One module is prepared for optical measurements, having circular observation windows on each side, where the transparent part has a 40 mm diameter.

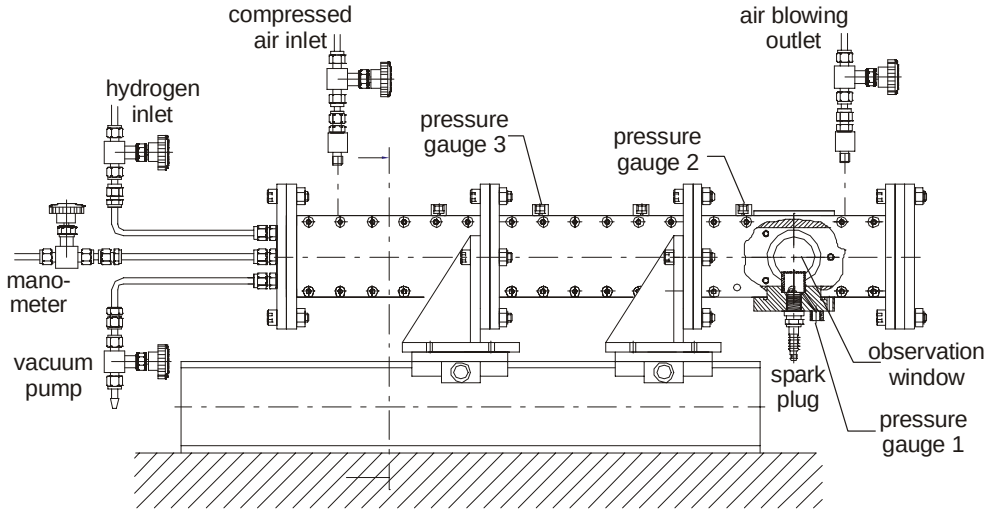

Figure 1. The combustion rig is composed of two standard modules (2 parts left) and one measuring module (right) with observation windows. In the configuration shown in the figure, pressure gauges and a spark plug is attached.

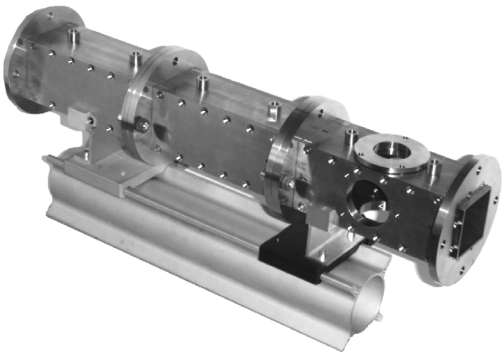

Figure 2. Photograph of the rig

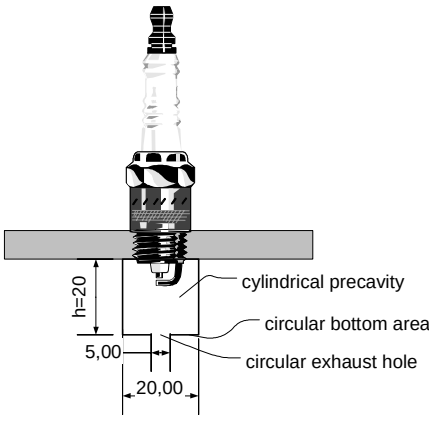

Figure 3. Ignition cavity.

3.2 Air/hydrogen flame jet experiment

In the experiment described here, one of the windows is replaced by a spark plug socket. The spark plug is mounted in a cylindrical cavity with a small exhaust hole, see figure 3. Three pressure gauges are used. One

measures the pressure inside the cylindrical cavity (gauge 1), while the other two (gauges 2-3), measures the pressure outside the cavity.

The rig is filled with a stoichiometric air/hydrogen gas mixture. After ignition an overpressure is built up in the cylindrical cavity, giving rise to a jet flame which propagates through the exhaust hole. The jet flame is studied using PLIF, schlieren and holographic interferometry. The time intervals between start of ignition and image recording were varied in a series of tests. In figure 4 a typical pressure registration is shown.

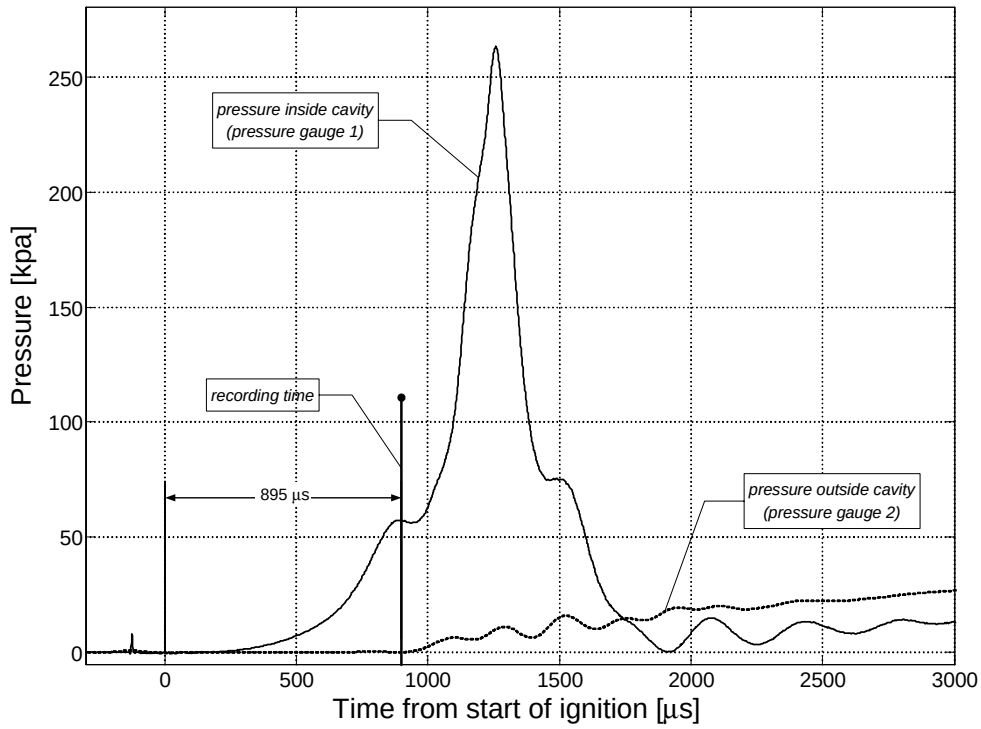

Figure 4. Typical pressure curve inside the rig.

4. Work on PLIF – Planar Laser Induced Fluorescence

4.1 Background

Planar laser induced fluorescence (PLIF) is mainly used for concentration measurements of single species. In a typical PLIF experiment a short pulse tunable narrow bandwidth laser is magnified by a cylindrical lens to a light sheet in a cross section of the flame (see figure 5). It induces an appropriate transition for the desired species (e.g. OH). Perpendicularly to the laser beam, an electronic image sensor records the fluorescence radiation through a filter, thereby selecting an appropriate fluorescence transition wavelength.

In the following the work done to develop the equipment and the experimental technique for FOI Grindsjöns PLIF system will be described.

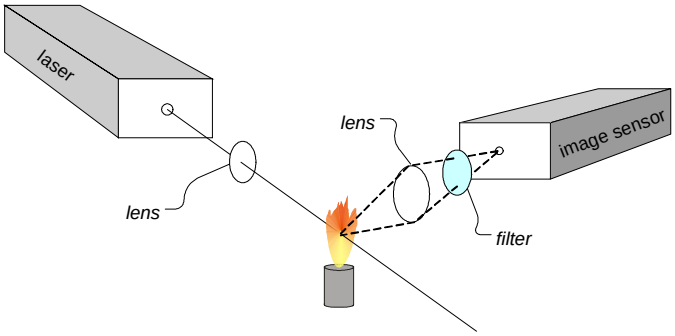

Figure 5. Schematic LIF set-up

4.2 Equipment

Lasers

The YAG-pumped DL-Midi dye laser that was originally used, has been replaced by an EXCIMER-pumped LPX dye laser from LAMBDA. The reason being the difficulty to adjust and optimize the old laser, and the trigging which was a potential problem for the YAG-system. The EXCIMER laser can be externally trigged which has simplified the triggering procedure considerably. The laser function is similar, with a dye lasing at 565.825 nm. The emitted light is frequency doubled in a BBO I crystal to 282.912 nm. The beam that leaves the crystal is a mixture of the original light and the doubled light. This light is being filtered instead of, as previously, led through a separating system of crystals. Filtering is a much simpler method.

While the dye used now, Coumarine 153, gives weaker lasing than the dye used before in the DL-Midi laser, this is to some extent compensated by the much more powerful EXCIMER laser pumping. The final output for each pulse is around 1 mJ, i.e. about the same as with the other laser.

Sensor and optics

In order to get a 2D distribution of the OH radical in the rig a fast trigged, high sensitive, camera with amplification is used as sensor. It is a Jobin Yvon CCD-3000i with an imaging area of 26.6×6.7 mm² (1024×256 pixels), with an optical system in front of it, see figure 6. It is sensitive for wavelengths in the interval 190–850 nm with a maximum amplifica-

tion of 18000 and a dynamic range of 125000:1. The shortest exposure time, or shutter time, is 100 ns. However, over the entire image area it operates better at 200 ns. The software for the camera is not up to date and there are problems with converting the images to a readable format for further image processing. This was overcome with a home-made program that converts the files. Due to the high gain used, occasional pixels will get high values from cosmic radiation and electronic noise. These pixels need to be filtered away. To remedy these things, routines for image processing were made in MATLAB. This has also made it possible to use image processing algorithms to enhance the images and to extract more information from the experiments. When better images have been produced, further improved filters and analysis methods will be developed.

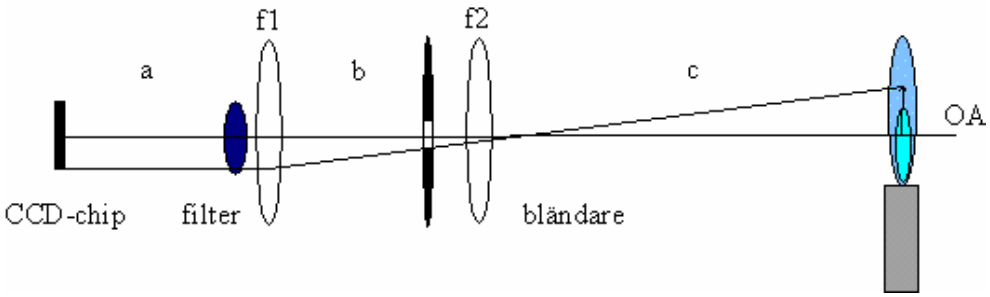

Figure 6: The imaging system used in the experimental rig. The focal lengths and distances are f_1 = +60 cm, f_2 = +8 cm. a=8 cm, b=8 cm and c=14 cm, resulting in a 4/7 magnification. Consequently, the windows of the rig (Ø = 4.7 cm) can be fully imaged onto the CCD-chip (width 2.66 cm).

The light emitted from the rig needs to be filtered to remove scattered light from the laser and the light from the combustion, while still letting the fluorescence through. A new filter with higher transmittance has been tested. The laser's wavelength is 282.912 nm, while the fluorescence we are interested in is at 310 nm. Until now, the interference filter 03 FIU 121 from Melles Griot has been used. The filter transmits around 310 nm, with a maximum transmittance of 18% near normal incidence, see figure 7 top. The new filter, CG-WG295-1.00 from Schott, transmits light with wavelengths longer than 305 nm with close to 100% transmittance, see figure 7 bottom. A possible problem when using this filter is that scattered light of longer wavelengths might interfere with the result.

To determine the moment of arrival of the laser pulse during the pressure rise, a photo detector, 10AP 488-1 from UDT, has been introduced into the setup. The detection is done under the rig. After the light has passed the two windows through the rig, it receives scattered light from a paper. The detector reacts very fast for incident light (a few nanoseconds rise time, see figure 8).

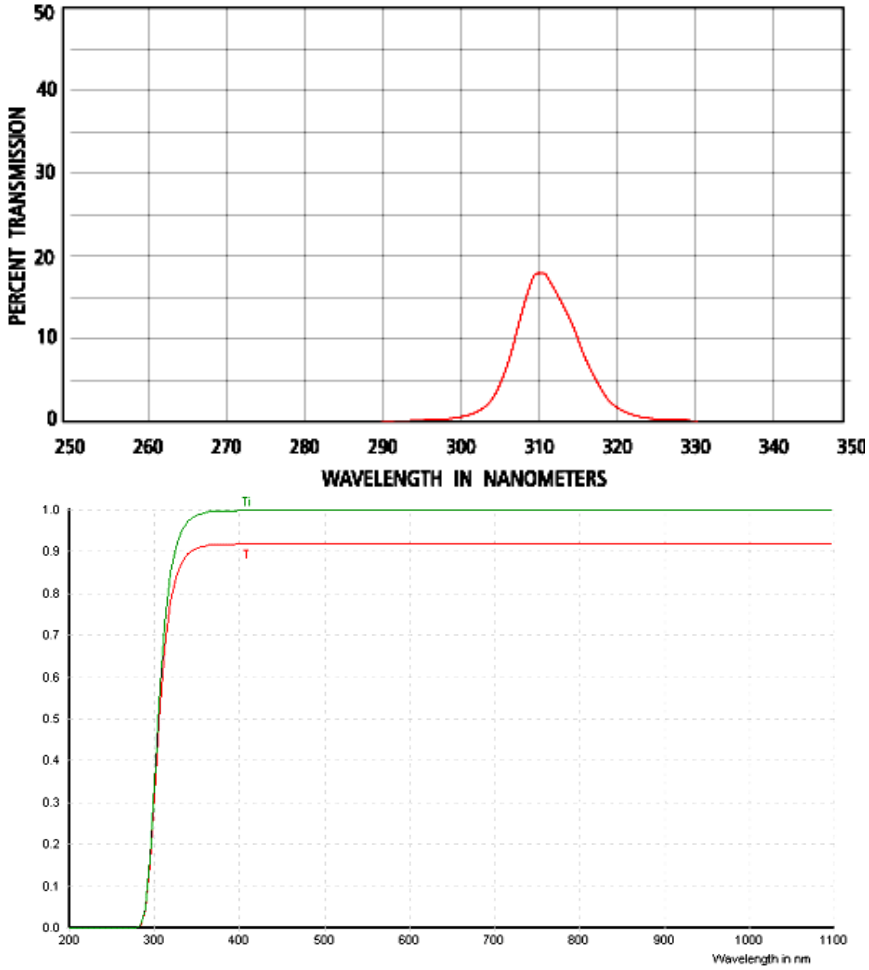

Figure 7: Transmission curves of the filters. The interference filter (top) and the high bandpass filter (bottom), with the overall transmittance in red.

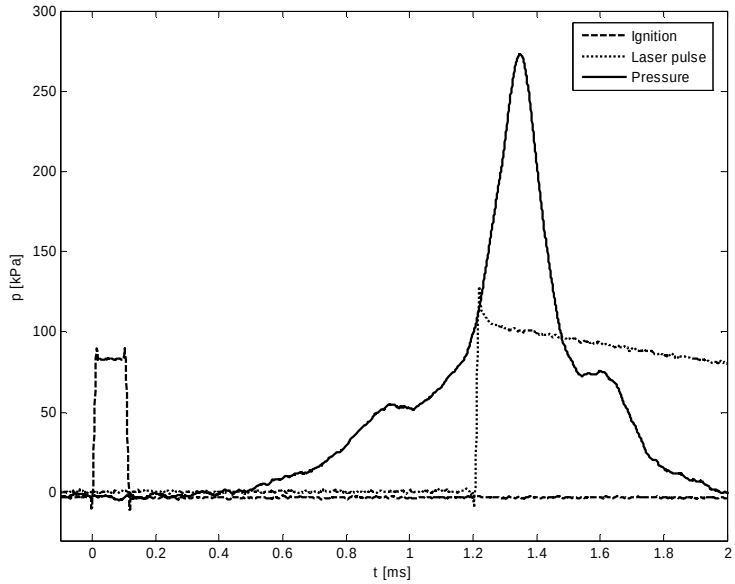

Figure 8: Oscilloscope read-out. It takes a few hundred microseconds for the pressure to build up in the rig. The durability of the laser pulse is a false artefact coming from the fluorescence on the paper the laser is reflected on. It is only 28 ns long.

To get a 2D image of a thin slice of the combustion zone, we use a set of planar optics from LaVision, see figure 9. It generates a light sheet of the laser beam that covers the whole area of the optical access window in the rig. It consists of a combination of two spherical lenses and a cylindrical lens, all made of quartz since normal glass does not transmit UV wavelengths.

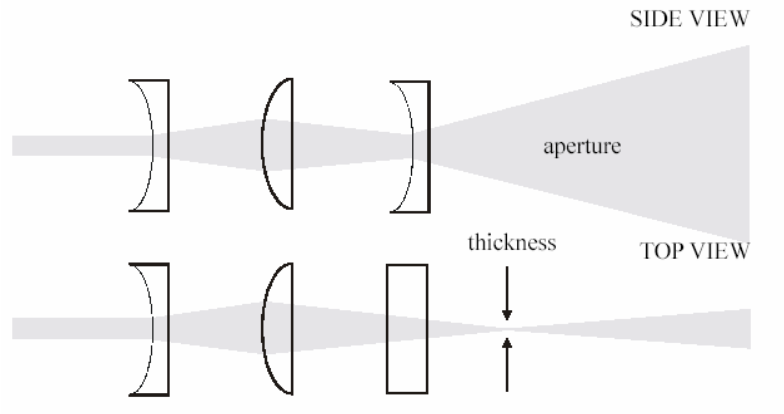

Figure 9: "Light Sheet Optics" from LaVision.

4.3 PLIF experiments in the combustion rig

The combustion rig is described in chapter 2. All events are controlled by the trig system, see figure 10. The laser pulse and the shutter of the camera need to be synchronised with the ignition of the gas mixture and the subsequent pressure rise. Since it can be trigged by a push of a button the entire trigging system has become less complicated than before.

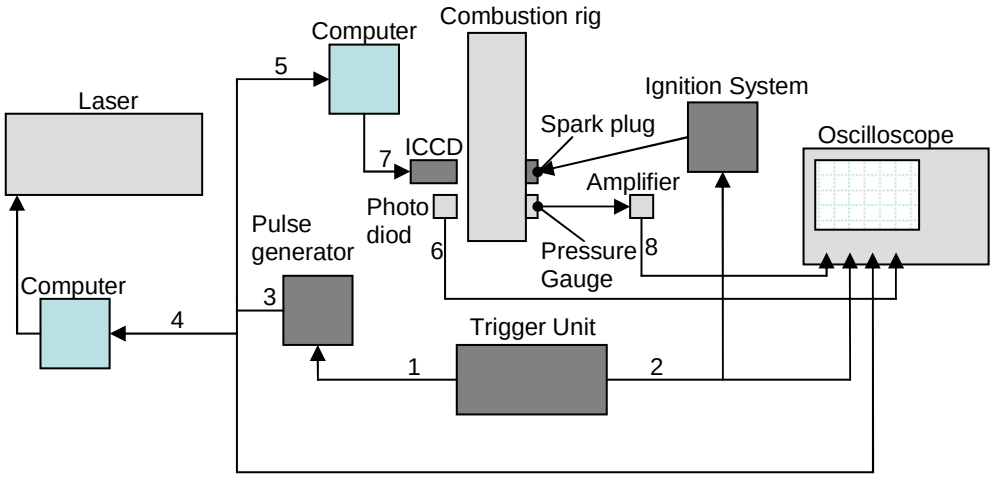

Figure 10: An outline of how the different parts of the system are connected for trigging.

After being initiated by the start signal, the system sends a pulse to the spark plug and to a Stanford DG535 pulse generator. The pulse generator will then send pulses to the pump laser and the camera, with adjustable delays. The delays are varied depending on when during the pressure rise an image should be captured, see figure 11.

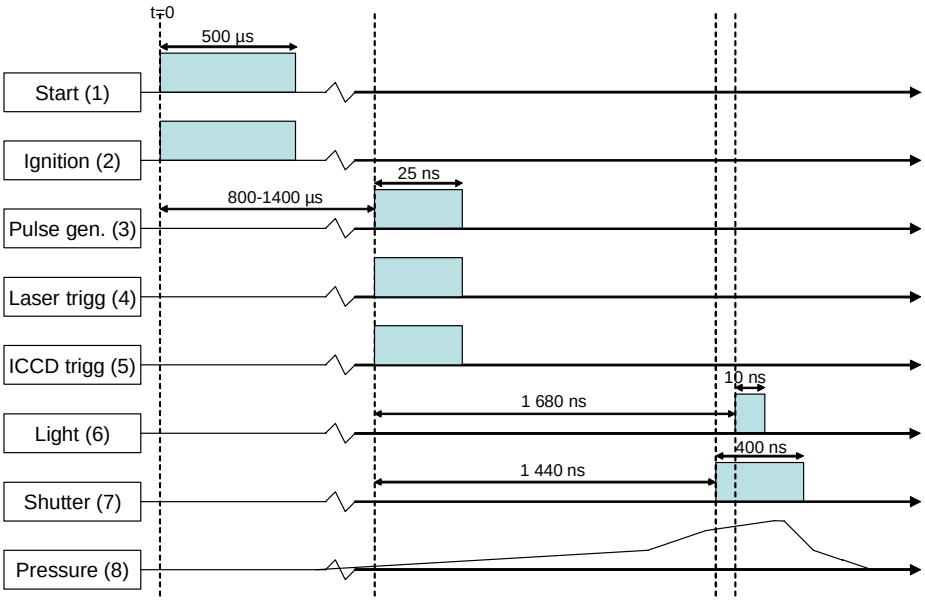

Figure 11: Time schedule for the entire process. The time increments are not in scale.

The planar laser beam enters the rig from the top window and leaves it through the bottom window, see figure 12. The camera views the ignition plug through a side window and will see the plume of combustion from the front, with the laser sheet covering more or less its entire view.

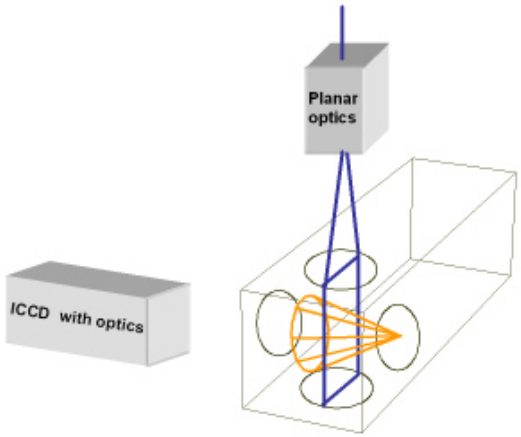

Figure 12: Schematic figure of the rig and the three quartz windows used.

In the first experiments, a control was made that the laser wavelength was correct by doing PLIF on a propane flame, where the wavelength was optimized for maximum output. This had to be done since the wavelength shown on the display of the dye laser is just an approximate. Several ignitions were made on hydrogen-air mixture in the rig, but so far we have not been able to image the fluorescence from OH. The only image, see figure 13, containing information so far, is one taken with the new high bandpass filter. However, it may be mainly scattering that has been imaged. In any case further experimental studies are needed to confirm what is really seen in the image.

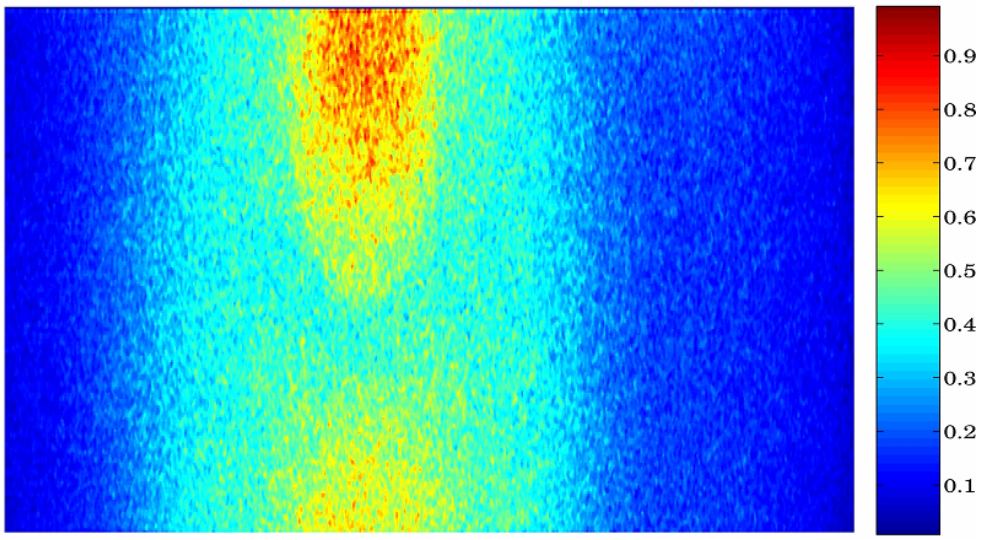

Figure 13: Image taken in the combustion rig with the high bandpass filter, the scale is normalized.

It can be questioned whether we have enough OH to detect any fluorescence. With good balance between the H_2 and O_2 concentrations, all H_2 might be too rapidly consumed. Because of this, measurements with less H_2 than needed for optimal combustion have been done, but to no avail. PLIF measurements on hydrogen-air mixtures are a commonly used technique, but it is usually done on an anchored flame. In these experiments OH is seen in the outskirts of the flame, diffusing into ambient air. We expected to see a similar OH distribution in our experiments. The difference is that OH will probably survive longer in air than in a mixture containing H_2, which consumes it very fast when H_2O is formed. It might be the case in our experiment, with combustion taking place in an atmosphere consisting of premixed fuel/air, giving OH very short life times, and therefore low concentration.

5. Work on interferometry and schlieren

5.1 Background

Interferometry and schlieren techniques were the first optical techniques used for the study of fluids. Both of these methods have their advantages and disadvantages. Interferometry gives best quantitative values. However, the result is usually given as phase maps, i.e. wrapped mod(2π), which presents an often unsolvable inversion problem, the so called "unwrapping problem". Another problem is the "speckle noise" due to the coherent light source. Schlieren can be made more sensitive and is superior as regards detection of small, dense variations (i.e. first derivatives) which can be hard to distinguish in an interferogram. One major problem with schlieren systems is the difficulty to quantify the results. The evaluation is based on measurement of contrast values over the images, which usually are influenced by noise, detector nonlinearities, diffraction and shadowing effects. A common disadvantage for both methods is that they give integrated results. To evaluate the true 3D refraction distribution, tomographic methods have to be used, except for some special situations. One is for very thin objects; another is for axially symmetric objects where Abels integral equation can be used.

In previous reports [5,6,8] we showed how Large Eddy Simulations (LES) were used to simulate interference patterns and schlieren images of the flame dynamics of turbulent propane-air jet flames using ray-tracing. By comparison to experimental schlieren images and phase maps obtained from pulsed TV holography, quantitative and qualitative (by counting fringes) validation of the LES-model could be carried through.

Here it will be demonstrated how schlieren and interferometry can be combined in order to utilize each techniques advantage. This work has been carried out in cooperation with Luleå University of Technology, Div. of Experimental Mechanics. Evaluation, calibration and Abel inversion algorithms for this purpose have been developed (see appendixes 2-5)). By comparing the techniques, their shortcomings and benefits becomes evident. The evaluation techniques have been tested on an experiment performed where a high speed turbulent flame jet was produced as described in chapter 2.

5.2 Experimental set-up

In figure 14 the schlieren system is shown. Collimated white light from a slit aperture, is deflected by optical inhomogenities introduced in the light path. The schlieren effect is produced by a knife edge placed in the back focal plane of the second schlieren lens. Compared to an undisturbed light path, some of the light that was blocked away will now pass the edge and vice versa.

The system has two identical aspherical lenses with diameter 110 mm and focal lengths f2=800 mm. The light source is a Xenon flash lamp that emits light pulses of 100 mJ during 3 μs. The images were recorded by an electronic digital camera with resolution 2000 ×1312 pixels , giving an image resolution of 45 μm/pixel.

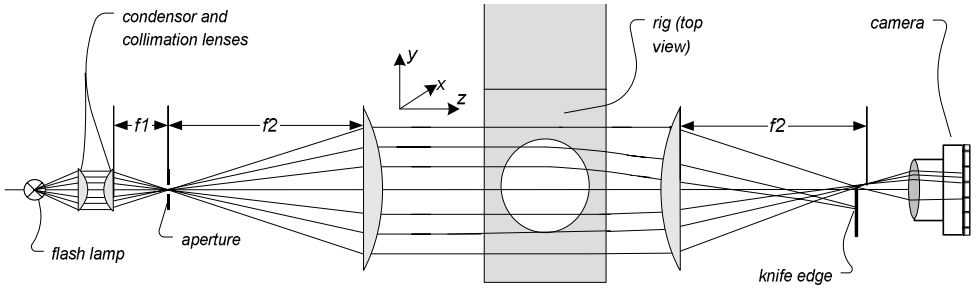

Figure 14. The schlieren system (the deflection angles are very exaggerated). To reduce chromatic aberrations, an additional red filter was placed in front of the light source.

In the experiments, one reference (background) image B_0 is recorded before ignition (but after the filling of gases), and a second image B at varied times after ignition. Using image processing, an estimate of the contrast image is then calculated to

$$\tilde{C} = \frac{B - B_0}{B_0}. \tag{1}$$

The interferometrical measurements were performed using an all-electronic version of holographic interferometry called pulsed TV holography [10,11]. The experimental set-up that has been used is shown in figure 15. Its principal components are a double-pulsed Q-switched ruby laser which can provide double pulses with time separation from 1 μs up to 800 μs and a CCD camera (PCO Sensicam, 1024×1280 pixels, each of size 6.7×6.7 μm², giving an image resolution of 37 μm/pixel) used to record image plane holograms at different states of the object (the jet flame). The set-up enables us to compare burning gas with undisturbed air or gas, burning gas at different short time intervals and non burning gas flow with undisturbed air.

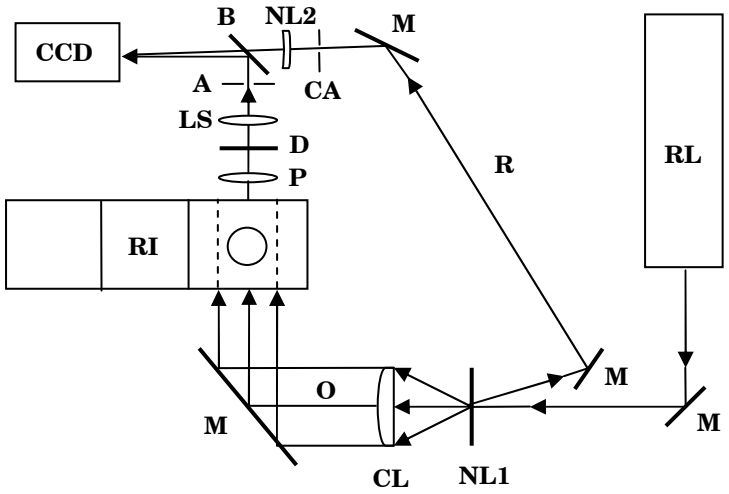

Figure 15. Experimental set-up, view from above. A: Rectangular aperture, B: Beam-splitter, CA: Circular aperture, CCD: CCD-detector, CL: Collimation lens, D: Diffuser, LS: Lens system, M: Mirror, NL1-2: Negative lenses, O: Object beam, P: Positive lens, R: Reference beam, RI: Rig, RL: Double-pulsed ruby laser.

Laser light with a wavelength of 694 nm is emitted by the double-pulsed ruby laser, RL. The duration of the pulse is about 30 ns. The main part of the emitted laser light is expanded by the plano-concave lens NL1, collimated by the lens CL and thereafter propagated through the phase object inside the rig, RI, and constitutes the object light, O. The lens PL images the phase object onto the diffuser D, thus reducing the speckle motion caused by the deflection of light rays due to changes of the refractive index gradient. This lens is also used to control the magnification of the object on the diffuser. The diffuser is imaged onto the CCD detector by the lens system LS. A small portion of light is reflected at the plane surface of NL1 and is used as the reference light R. The object light and the tilted reference light interfere at the CCD-detector. A rectangular aperture A in the imaging system reduces the spatial frequencies to be resolved by the detector.

Two different states of the object are compared interferometrically and a phase map [10,12] is calculated, by using the Fourier transform method [13], representing the integrated phase difference in optical path length mod(λ), where λ=694 nm is the laser wavelength.

5.3 Experimental results

In figures 17-20 some experimental results are shown, showing schlieren contrast images and wrapped interferometric phase maps recorded at equal times (700-1000 μs) after start of ignition. Even if the combustion process is not fully reproducible, the images show striking similarities. The pressures inside the cylindrical cavity at the times of recording are given in table 1.

Table 1. Measured pressures inside the cylindrical cavity at the times of recording.

Time (μs)	Pressure schlieren (kPa)	Pressure interferogram (kPa)
700	125	123
800	146	155
900	166	157
1000	159	159

Figure 17-20 show the jet flame propagation at different instants. A white spot is clearly seen in the phase map in figure 17 which is probably a projection of a vortex ring (a so called smoke ring). In the schlieren image it is not obvious that it is a “smoke ring” that appears, while the edges of the jet flame, which are invisible in the interferogram, are clearly distinguishable. This demonstrates the advantages and disadvantages of the methods, i.e. the ability of schlieren to detect small gradients and of interferometry to detect small differences in pathlength. In figure 18 a jet flame is visible in both the schlieren image and the phase map. The jet flame has started to ignite the surrounding gas mixture. The ignited area shows a turbulent structure. There is a gap in the lower section of the jet flame in the phase map that is not seen in the schlieren image. The “smoke ring” is still visible and has propagated further. In

figure 19 the ignited area is expanded and has reached the top of the observation window and its upper section is burning in a turbulent manner. The “smoke ring” is no longer visible. In figure 20 the burning area has grown even further and the turbulent structure is intensified. A plume is seen at the top of this region that might be caused by reflections inside the rig. The jet flame is shorter and wider.

The images were then evaluated according to the methods described in appendixes 2-4. The schlieren images were calibrated according to eq.(11) in appendix 2 by comparing the refraction index difference in the unwrapped phase map with the integrated schlieren images for the lower 4 mm part in the jet flame (i.e. below the turbulent part) after 900 μs. The maximum values of the pathlength differences along the jet flame were least-square fitted to each other. The relative spread of the calibration was 3,8% (one standard deviation). Figure 16 shows the calibrated profiles. In figures 21-23, the integrated schlieren images and unwrapped phase maps are shown. The colorbars should be interpreted as reduction of refraction index. If the integrated schlieren and unwrapped phase maps are compared, the results are similar both as regards magnitude of path differences and jet flame shape. In figure 21 e.g. the white spot is now clearly seen in the integrated schlieren image as well as in the unwrapped phase map.

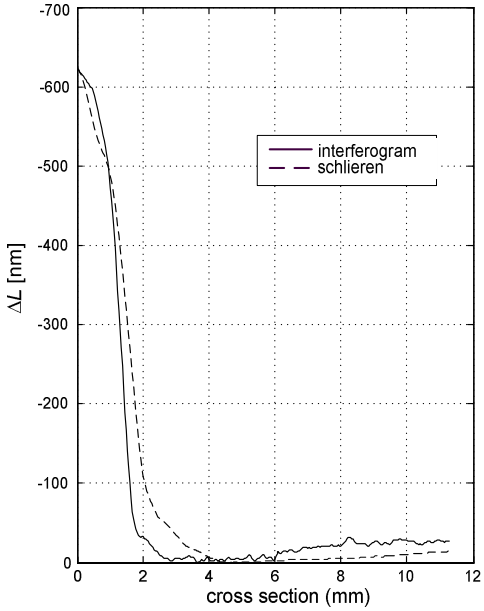

Figure 16. Resulting profiles after calibration.

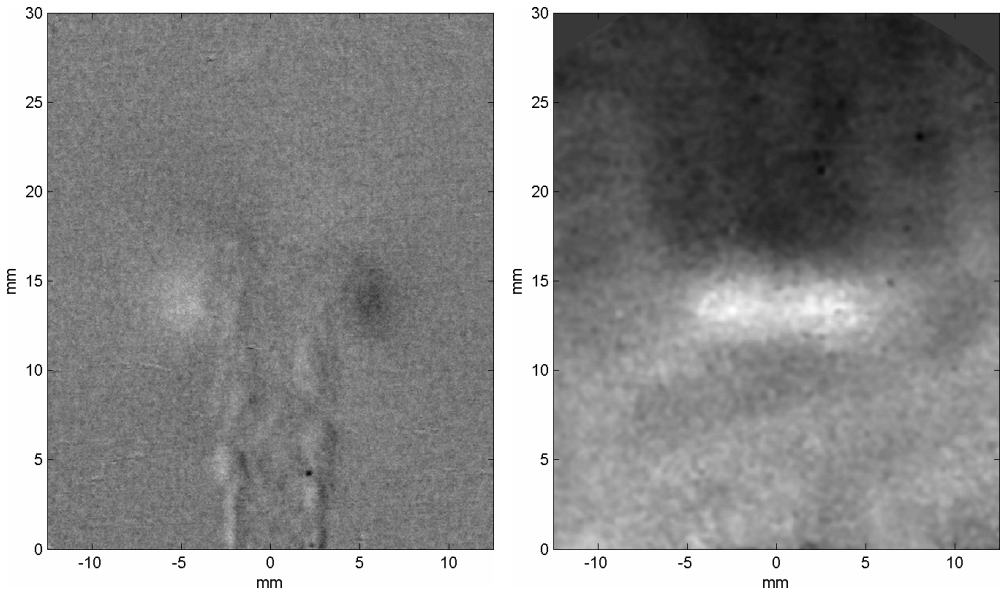

Figure 17. Schlieren image (left) and interferometric phase map (right) 700 µs after ignition start.

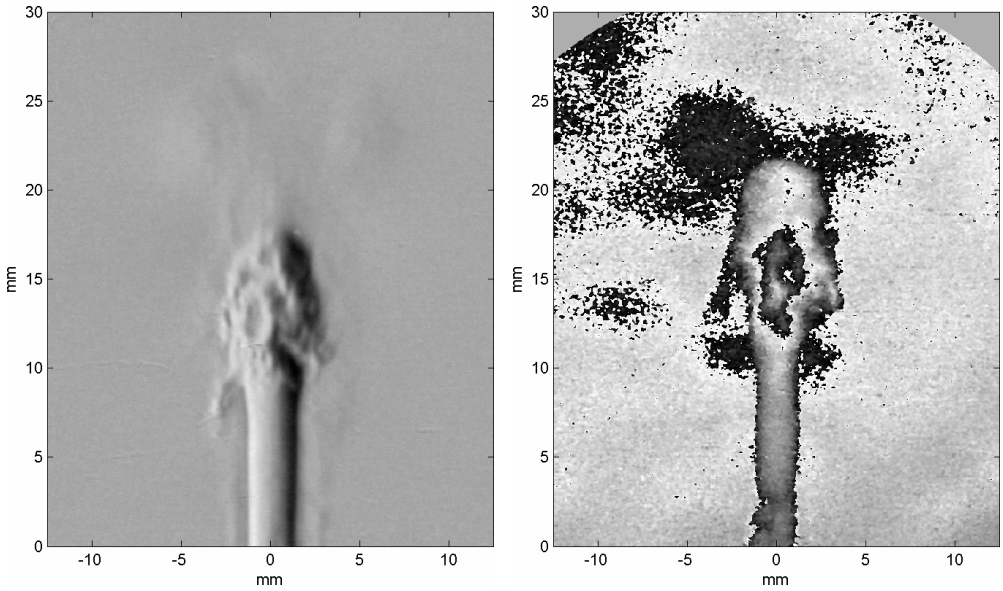

Figure 18. Schlieren image (left) and interferometric phase map (right) 800 µs after ignition start.

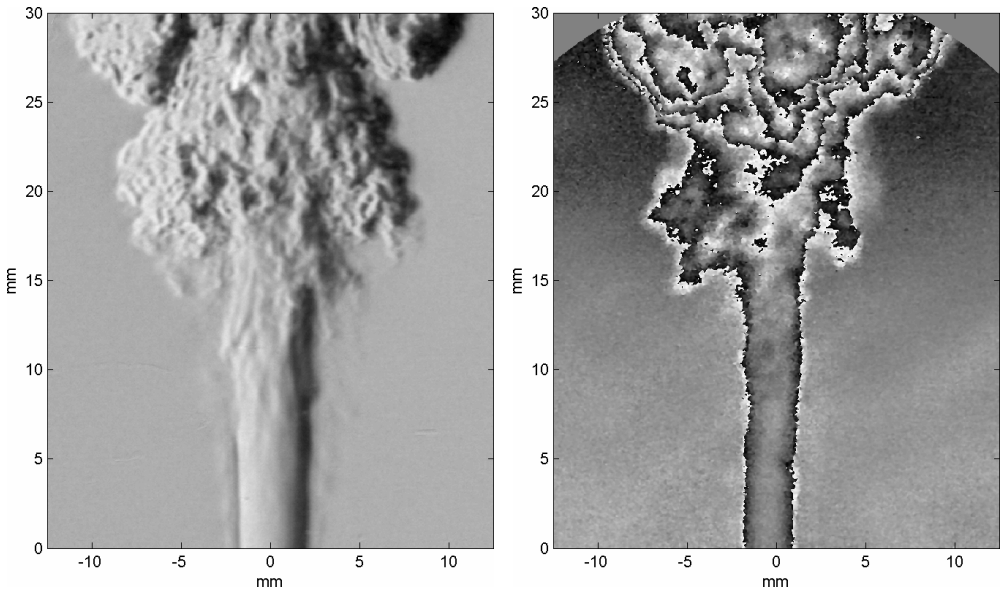

Figure 19. Schlieren image (left) and interferometric phase map (right) 900 µs after ignition start.

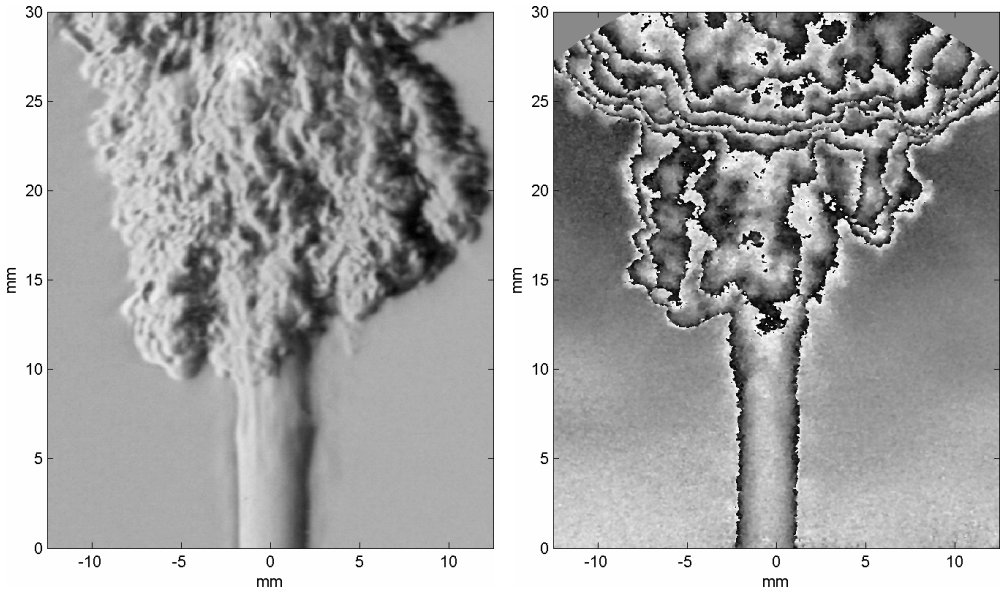

Figure 20. Schlieren image (left) and interferometric phase map (right) 1000 µs after ignition start.

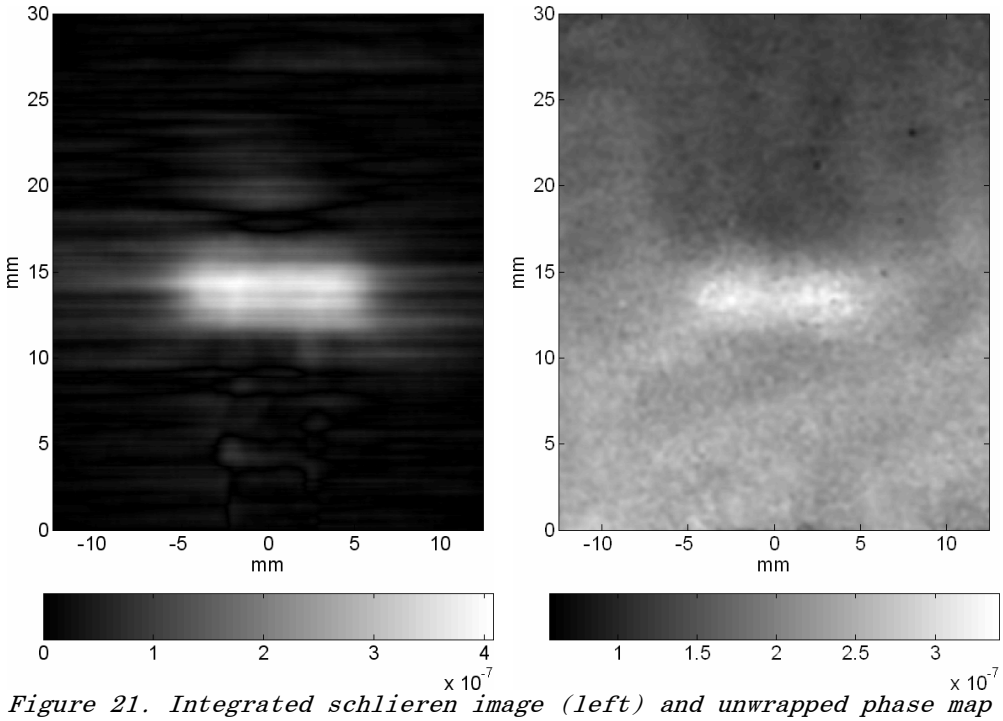

Figure 21. Integrated schlieren image (left) and unwrapped phase map (right) 700 µs after ignition start. The colorbar shows the path-length difference in meter.

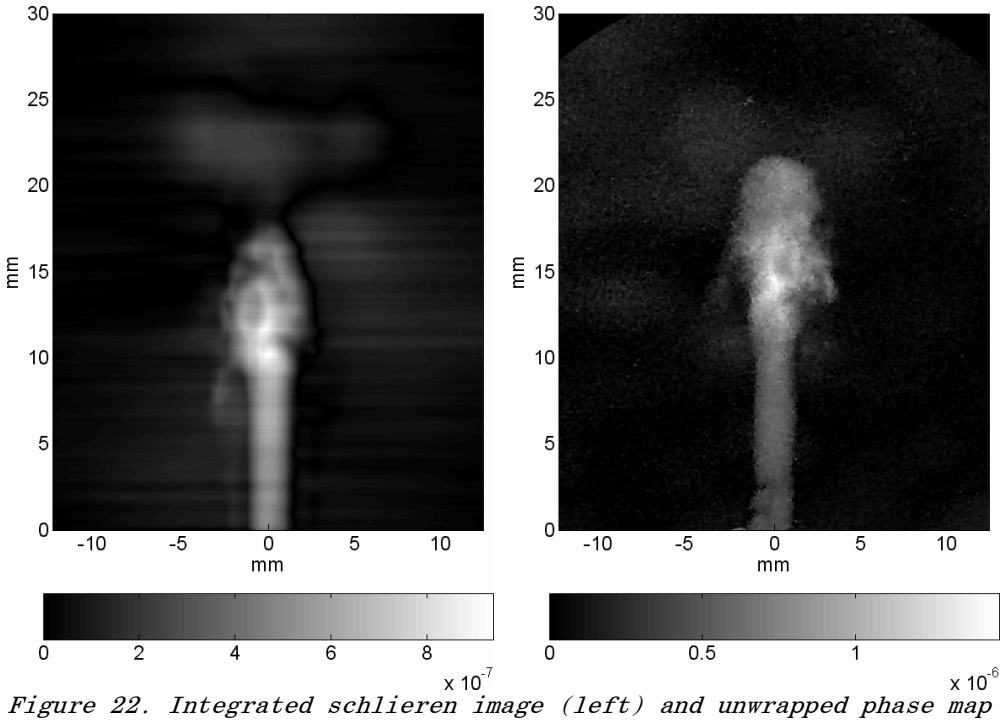

Figure 22. Integrated schlieren image (left) and unwrapped phase map (right) 800 µs after ignition start. The colorbar shows the path-length difference in meter.

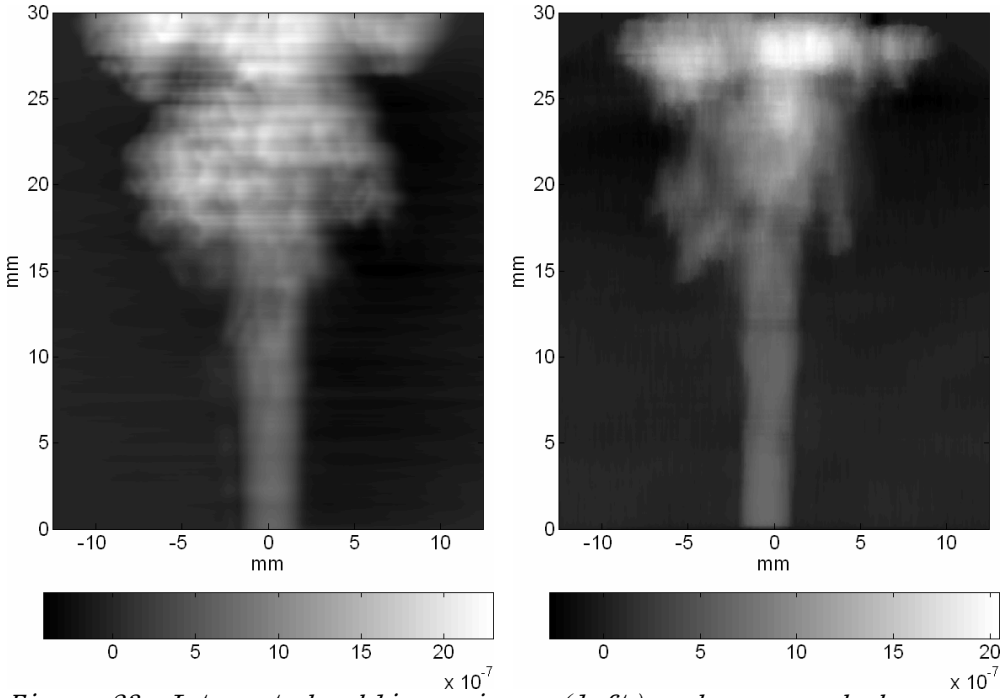

Figure 23. Integrated schlieren image (left) and unwrapped phase map (right) 900 µs after ignition start. The colorbar shows the path-length difference in meter.

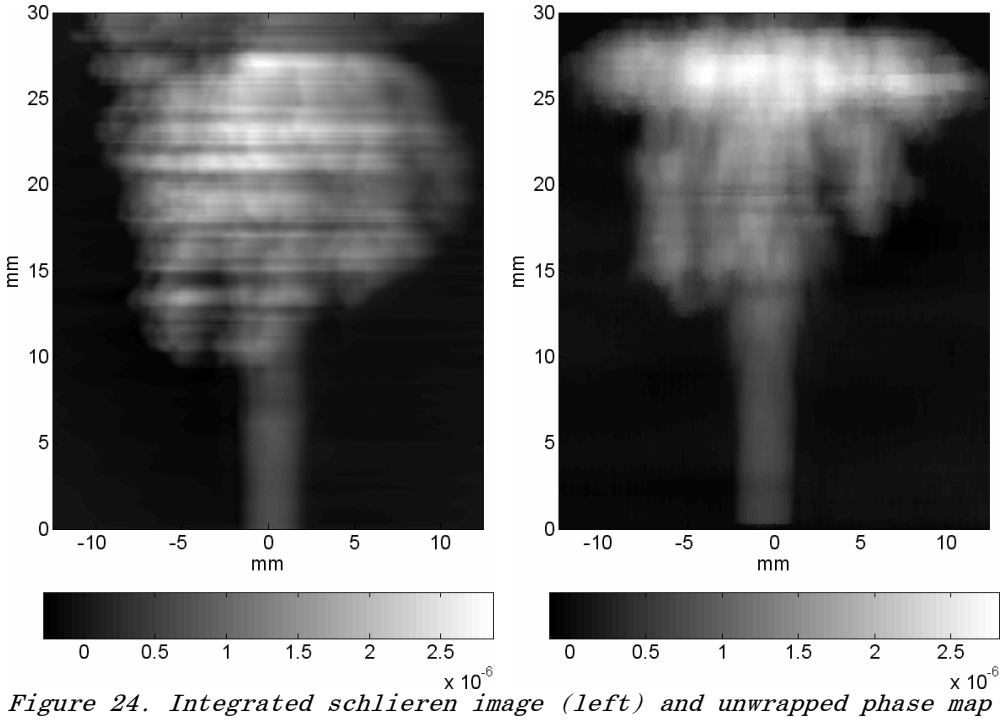

Figure 24. Integrated schlieren image (left) and unwrapped phase map (right) 1000 µs after ignition start. The colorbar shows the path-length difference in meter.

Using these results, the radial profile of the refraction index for the lower (axially symmetric) part of the jet flame was evaluated using Abel inversion according to appendix 5. Figure 25 shows the mean values of the radial refractive index between 0-10 mm up to 4 mm above the outlet of the jet flame calculated from the schlieren and pulsed TV holography results 800 μs and 900 μs after ignition start. Even here the results are similar for both schlieren and interferometric measurements. However, the schlieren measurement gives less change in refraction index, the lower peaks seem to be topped off. This can not be explained by the small difference in image resolution, but is probably due to the better ability of interferometry to resolve small changes in optical pathlength.

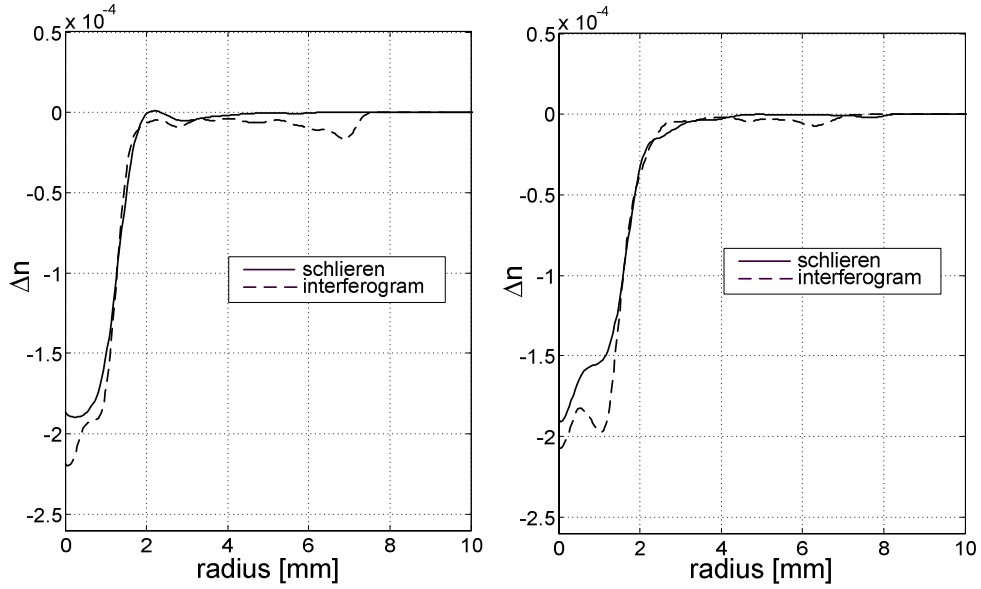

Figure 25. Cross sections of the refractive index fields, calculated from the schlieren and pulsed TV holography results using the Abel-transformation. The profiles are obtained from data 800 μs (left figure) respectively 900 us (right figure) after the ignition start.

The densities can now be calculated using eq. (5) in appendix 1. If it is presumed that the gas inside the flame is fully combusted, the reaction is described by:

$$2H_2+O_2+3.74N_2+0.04Ar \rightarrow 2H_2O+3.74N_2+0.04Ar\ ,$$

where the mass fractions (Y) for the original mixture are

$$Y_{H_2} \approx 2.8\%,\ Y_{Air} \approx 97.2\%\ \left(Y_{O_2} \approx 22.4\%,\ Y_{N_2} \approx 73.6\%,\ Y_{Ar} \approx 1.1\%\right)$$

and for the reaction products

$$Y_{H_2O} \approx 25.3\%,\ Y_{N_2} \approx 73.6\%,\ Y_{Ar} \approx 1.1\%\ .$$

Using eq.(6) in appendix 1, the mixing properties become according to table 2. The densities become accordingly,

$$\rho = \frac{n-1}{K} = \frac{\Delta n + n_{H2/Air} - 1}{K_{H2O/N2}} = \frac{\Delta n + 2.44 \cdot 10^{-4}}{2.4 \cdot 10^{-4}}\ . \qquad (2)$$

Table 2. Properties of involved gas mixtures.

Mixture	Gladstone-Dale constant, (m^3/kg)	Density, (kg/m^3)	Refraction index NTP, (n-1)
Original (H2/air)	$2.60 \cdot 10^{-4}$	0.94	$2.44 \cdot 10^{-4}$
Reaction products (H20/N2)	$2.37 \cdot 10^{-4}$	1.10	$2.60 \cdot 10^{-4}$

A rough temperature estimate can be achieved using the ideal gas law, if constant pressure is assumed across the jet flame,

$$T = \frac{\rho_0}{\rho} T_0 = \frac{2.61 \cdot 10^{-4}}{\left(\Delta n + 2.44 \cdot 10^{-4}\right)} T_0 , \tag{3}$$

where $T_0 = 293\,\mathrm{K}$ is the ambient temperature.

The uncertainty of the temperature estimate u_T becomes very sensitive to the measurement uncertainty $u_{\Delta n}$ of the index of refraction change according to

$$u_T \approx \left|\frac{dT}{d(\Delta n)}\right| u_{\Delta n} = \frac{2.61 \cdot 10^{-4} T_0}{\left(\Delta n + 2.44 \cdot 10^{-4}\right)^2} u_{\Delta n} . \tag{4}$$

In figure 26 the relation between temperature and refraction index change, including limits for 5% uncertainty of refraction index change. As can be seen, for high temperatures even small uncertainties give rise to large temperature estimation uncertainties. In the centre of the flame, the measurements give a $\Delta n \approx 2.0 \cdot 10^{-4}$ resulting in a temperature of approximately 1700 K. A typical uncertainty for interferometrical measurements is around ±5%, resulting in an temperature uncertainty between 1400 -2200 K according to the figure.

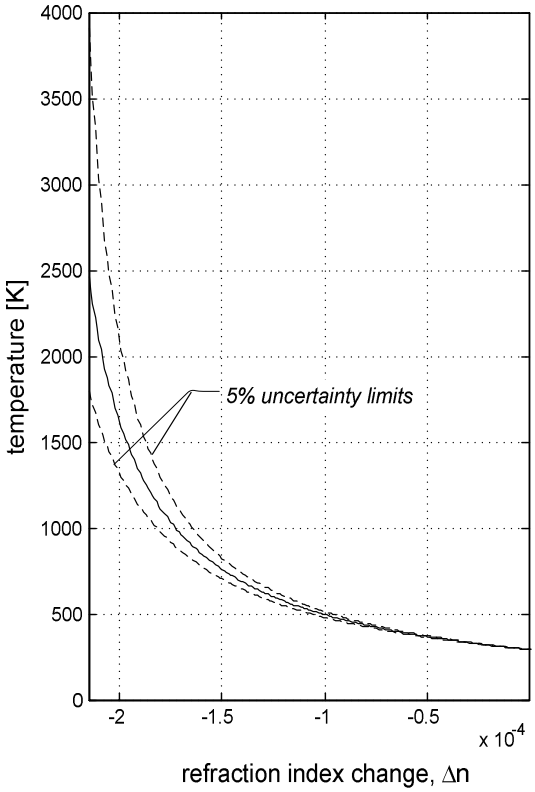

Figure 26. Relation between temperature and refraction index change, including limits for 5% uncertainty of refraction index change. For high temperatures even small uncertainties give rise to large temperature estimation uncertainties.

6. Conclusions and discussion

The most important conclusions that can be drawn from the work described in this report are:

- By changing laser and improving the trig system as well as other experimental equipment and technique, PLIF has now been a useable method.
- It has been demonstrated how schlieren and interferometry can be combined in order to utilize each techniques advantage.
- The algorithms which have been developed for this purpose as well as for evaluation of three-dimensional density profiles using the Abel transform, have shown to work well.

This autumn, when the LIF work was scheduled, the laser lab was not available during three months due to much delayed reconstruction works. Due to this and problems with equipment, etc., the PLIF experiments are lagging. After the construction was finished in October, some progress has however been made. Several of the previous problems have been rectified and a step-by-step approach is used, making it easier to track down potential problems along the way, giving possibilities to perform a number of experiments next year.

The schlieren and interferometry techniques have been further developed, compared and combined. These techniques have still a great potential of development although they have been used during a long period of time. This is mainly due to the development of improved equipment such as electronically detectors and light sources and the access to high performance computer-based evaluations. One advantage with the schlieren method compared to the pulsed TV holography method is that obtained gradients are smoother and contains less speckle noise. However, the schlieren results can be calibrated using interferograms generated by pulsed TV holography. Although the combustion process is not fully reproducible the results obtained from each technique show striking similarities.

7. Future work

Further development of the PLIF system is needed to give useful images. Other fuels than H_2 will be tested in the rig, for example propane, to see if a more complicated and slower combustion process gives higher concentrations of OH. Quenching, where the OH relax through collisions and without emitting fluorescence, might also be problem. The higher the pressure, the more quenching will take place, due to more collisions. In order to reduce the quenching, experiments giving lower pressure will be performed.

The results obtained from schlieren and interferometry experiments are expected to be useful for examination of and validation of numerical models describing combustion processes. Hence our intention is to continue with further combustion experiments as well as development and evaluation of CFD-models, using ray-tracing, to describe the combustion process. The experimental methods used for validation can be developed further to get more quantitative information from combustion processes and ignition events by combining them with other methods. A promising method is to combine pulsed TV holography with the new method of defocused speckle photography, which is a method to obtain quantitative data about phase objects such as flames with non-uniform refractive index and thus density distributions.

Acknowledgement

The authors whishes to thank R. Mattsson and P. Gren at Luleå University of Technology, Div. Experimental mechanics, who participated in the work presented in chapter 4.

Appendix 1. Relation between refraction index and density

The variation of refraction index depends on the gases involved, pressure and temperature. For gaseous media the index of refraction is mainly decided by the density according to

$$(n-1)/\rho = K \tag{5}$$

where n is the index of refraction, ρ is the density and K is the Gladstone-Dale constant, which depends on the type of gas and the wavelength of the light. For a gas mixture, the Gladstone-Dale constant

$$K = \sum_{i=1}^{k} Y_i K_i \,, \tag{6}$$

where Y_i is the mass concentration and K_i is the Gladstone-Dale constant for gas i.

Table A1. Some values for Gladstone-Dales constant, λ =589.3 nm.

Gas	**K (m^3/kg)**	**Gas**	**K (m^3/kg)**
He	$1.95 \cdot 10^{-4}$	N_2	$2.38 \cdot 10^{-4}$
Ne	$0.74 \cdot 10^{-4}$	O_2	$1.90 \cdot 10^{-4}$
Ar	$1.58 \cdot 10^{-4}$	H_2O	$2.49 \cdot 10^{-4}$
Kr	$1.14 \cdot 10^{-4}$	CO_2	$2.27 \cdot 10^{-4}$
H_2	$15.4 \cdot 10^{-4}$	Cl	$2.37 \cdot 10^{-4}$

Appendix 2. Relations between schlieren and interferometry

Schlieren imaging is sensitive for deviations taking place perpendicular to the knife edge orientation. Suppose that the edge is oriented in the x-direction, and that the light propagates in the z-direction, see figure 14. (For reasons of simplicity, in the following all derivations are limited to deviations in the y-direction. Extensions to the x-direction are trivial). The deviation in the y-direction ε_y due to changes of the refraction index $n \approx 1$, can be estimated to [14,15]

$$\varepsilon_y(y) = \frac{1}{n_0}\int_0^L \frac{\partial n(y,z)}{\partial y} dz, \tag{7}$$

where L is the total optical path length and n_0 is the ambient refraction index. The deviation is proportional to the image contrast C according to

$$C(y) = \frac{E(y) - E_0(y)}{E_0(y)} = \frac{f}{h}\varepsilon_y(y) \tag{8}$$

where E and E_0 are the illuminances for images with and without the inhomogenity present, f is the focal length of the second schlieren lens and h is the height of the illuminated focal area which is not blocked away by the edge.

In interferometry, the difference in optical pathlength ΔL along the y-direction is measured according to [16,17]

$$\Delta L(y) = \frac{\lambda}{2\pi}\phi(y) = \int_0^L \left(n(y,z) - n_0\right) dz \tag{9}$$

where ϕ is the phase and λ is the wavelength of the light.

The relation between the interferometric and schlieren measurement can be found by integrating eq.(7) along the y-direction and changing the integration order and combining it to eq.(9),

$$\begin{aligned} \int_0^y \varepsilon_y(y)\,dy &= \frac{1}{n_0}\int_0^y\int_0^L \frac{\partial n(y,z)}{\partial y} dz\,dy = \frac{1}{n_0}\int_0^L\int_0^y \frac{\partial n(y,z)}{\partial y} dz\,dy \\ &= \frac{1}{n_0}\int_0^L \left(n(y,z) - n_0\right) dz = \frac{1}{n_0}\frac{\lambda}{2\pi}\phi(y) \end{aligned}, \tag{10}$$

that is

$$n_0\int_0^y \varepsilon_y(y)\,dy = \frac{\lambda}{2\pi}\phi(y)\ , \tag{11}$$

which can be used to calibrate the schlieren measurements if the phase change is measured using interferometry.

Appendix 3. Evaluation of schlieren images

In the schlieren experiments, one reference image B_0 is recorded before the event of interest takes place and a second image B during the event. Using image processing, an estimate of the contrast image is calculated to

$$\tilde{C} = \frac{B - B_0}{B_0}. \tag{12}$$

Using eq.(8) and knowing the focal length and edge area, quantitative values for the deviation could now be calculated which in turn could be integrated to find out the integrated index of refraction according to eq.(11). However, the recording process is far from ideal, nonlinearities and other influences will make quantification difficult. As is well known, when integrating experimental data, even small influences will deteriorate the result. In our case, due to the boundary conditions, the total phase change when integrating cross the jet flame should equal zero (since the integral goes from and back to an undisturbed background). The standard method for considering this is to subtract the mean value from the integral, but this is not applicable here, since we have a contrast image where the zero level is quite certain (i.e. $\tilde{C} = 0 \Leftrightarrow C = 0$). The following model can be used, which fulfills the conditions. Suppose that the effect of the influences can be modeled by

$$C(y) \approx a_1 \tilde{C}(y) + a_2 \left| \tilde{C}(y) \right|, \tag{13}$$

where $|..|$ denotes the absolute value.

The mean value of C across the jet flame should be zero, i.e.

$$\overline{C} \approx \overline{a_1 \tilde{C} + a_2 \left| \tilde{C} \right|} \Rightarrow \frac{a_2}{a_1} = -\frac{\overline{\tilde{C}}}{\overline{\left| \tilde{C} \right|}}, \tag{14}$$

where the top bars denote average values across the y-direction. By combining eqs. (8) and (14), the result becomes

$$\varepsilon_y = \frac{h}{f} C(y) \approx k \left(\tilde{C}(y) + \frac{a_2}{a_1} \left| \tilde{C}(y) \right| \right), \tag{15}$$

where the constant $k = a_1 h / f$ has to be found out by calibration with e.g interferometrical data.

Appendix 4. Phase unwrapping of interferograms

One disadvantage for interferometry is that the phase change is usually achieved mod(2π), i.e. wrapped, which has to be unwrapped. Suppose that the real phase change is $\phi(y)$. The wrapped phase $\tilde{\phi}(y)$ is

$$\tilde{\phi}(x,y) = \phi(x,y) + m2\pi \tag{16}$$

where m is an integer. The goal for the unwrapping is to find out which m should be added to different parts of the phase map. However, to find the Abel transform, the phase map does not have to be unwrapped. This is achieved by writing the derivative of $\exp(i\phi)$ in two different ways [24],

$$\begin{aligned} &\frac{d\left(e^{i\phi}\right)}{dy} = i\frac{d\phi}{dy}\cdot e^{i\phi} = \frac{d}{dy}(\cos\phi + i\sin\phi) \\ &\Rightarrow \frac{d\phi}{dy} = \frac{\frac{d(\cos\phi)}{dy} + i\frac{d(\sin\phi)}{dy}}{-\sin\phi + i\cos\phi} = \cos\phi\frac{d(\sin\phi)}{dy} - \sin\phi\frac{d(\cos\phi)}{dy} \end{aligned} \quad . \tag{17}$$

Now, even if $\tilde{\phi} \neq \phi$, $\cos\tilde{\phi} = \cos\phi$ and $\sin\tilde{\phi} = \sin\phi$, i.e.

$$\frac{\mathrm{d}\phi}{\mathrm{dy}} = \cos\tilde{\phi}\frac{\mathrm{d}\left(\sin\tilde{\phi}\right)}{\mathrm{dy}} - \sin\tilde{\phi}\frac{\mathrm{d}\left(\cos\tilde{\phi}\right)}{\mathrm{dy}} \tag{18}$$

and

$$\frac{\mathrm{d}^2\phi}{\mathrm{dy}^2} = \cos\tilde{\phi}\frac{\mathrm{d}^2\left(\sin\tilde{\phi}\right)}{\mathrm{dy}^2} - \sin\tilde{\phi}\frac{\mathrm{d}^2\left(\cos\tilde{\phi}\right)}{\mathrm{dy}^2}. \tag{19}$$

That is, if the sine and the cosine of the wrapped phase map are Savitzky-Golay filtered, eqs.18-19 can be used to find out the derivatives, which in turn can be directly integrated to unwrap the phase or used to calculate the Abel transform.

Appendix 5. Numerical evaluation of the Abel transform

In the case of axial symmetry the Abel transform [19] can be used to evaluate the 3D-refraction index field. If eqs. (7) and (9) are transformed to cylindrical coordinates, then

$$\varepsilon_y(y) = \frac{2}{n_0}\int_y^R \frac{\partial n(r)}{\partial r}\frac{r}{\sqrt{r^2-y^2}}dr \tag{20}$$

and

$$\Delta L(y) = \frac{\lambda}{2\pi}\phi(y) = 2\int_y^R \left(n(r)-n_0\right)\frac{r}{\sqrt{r^2-y^2}}dr\,. \tag{21}$$

These equations have inversions,

$$\frac{n(r)-n_0}{n_0} = -\frac{1}{\pi}\int_r^R \varepsilon_y(y)\frac{dy}{\sqrt{y^2-r^2}} \tag{22}$$

and

$$n(r)-n_0 = -\frac{\lambda}{2\pi^2}\int_r^R \frac{d\phi(y)}{dy}\frac{dy}{\sqrt{y^2-r^2}}. \tag{23}$$

These functions have to be numerically calculated. The evaluation involves two main difficulties; The singularity for $y=r$ and the differentiation of noisy empirical data. Here this is done by a variant of the "three-point Abel deconvolution" [20], by dividing the integral into partial sums,

$$\int_r^R \phi'(y)\frac{dy}{\sqrt{y^2-r^2}} = \sum_{r_i=r}^{R}\int_{r_i}^{r_{i+1}} \phi'(y)\frac{dy}{\sqrt{y^2-r^2}}\,, \tag{24}$$

where $\phi'(y) = \dfrac{d\phi(y)}{dy}$ and $r_{i+1} = r_i + \Delta r$. The singularity is avoided by Taylor expanding and integrating the partial sums

$$\int_{r_i}^{r_{i+1}} \phi'(y)\frac{dy}{\sqrt{y^2-r^2}} \approx \tilde{\phi}'\left(r_{i+1/2}\right)\left[\ln\left(y+\sqrt{y^2-r^2}\right)\right]_{r_i}^{r_{i+1}}\,, \tag{25}$$

where $\tilde{\phi}'\left(r_{i+1/2}\right)$ is an estimate of the derivative around $r_{i+1/2} = r_i + \Delta r/2$, and $\phi'(0) = 0$ by definition since the Abel transform is an even function.

The estimate of the derivative is found using the Savitzky-Golay technique of simplified least squares [21,22], which is based on performing a least squares linear regression fit of $\phi(y)$ to a polynomial of degree p>k over at least p+1 data points around each point to smooth the data. The derivative of order k is then estimated as the k:th derivative of the fitted polynomial at each point (for k=0 a smoothed curve is achieved). In the case of interferometry the first derivative is estimated, in the case of schlieren, the "zero:th" derivative is estimated.

References

[1] R. J. Goldstein (editor), Fluid mechanics measurements, Taylor & Francis, Washington, D.C. ,1996.

[2] O. Launilla , ”Förbränningsdiagnostik med laserinducerad fluorescens på OH-radikalen. En litteraturstudie,” FOA-R--00-01665-310—SE, 2000

[3] T. Carlsson, ”Utveckling av experimentella tekniker och experiment-anläggning för förbränningsstudier,” FOA-R--00-0-01608-310—SE, 2000

[4] T. Carlsson, ”Utveckling av experimentella tekniker och experiment-anläggning för förbränningsstudier, del II” FOI-R--0306--SE, 2001

[5] C. Fureby, T. Carlsson, M. Kupiainen, ”High Speed Combustion: Computational Fluid Dynamics Modeling and Experimental Diagnostics,” FOI-R--0520--SE, 2002

[6] T. Carlsson, ”Utveckling av experimentella tekniker och experiment-anläggning för förbränningsstudier, del II” FOI-R--0889--SE, 2003

[7] S. Wallin, M. Norrefeldt, M. Elfsberg, ”Förbränningsdiagnostik med laser-inducerad fluorescens på OH-radikalen”, FOI-R--1071—SE, 2003

[8] R. Mattsson, M. Kupiainen, P. Gren, A. Wåhlin, T. Carlsson and C. Fureby, “Pulsed TV Holography and Schlieren Studies, and Large Eddy Simulations of a Turbulent Jet Diffusion Flame,” Combustion and Flame, **139**, p.1-15, 2004.

[9] T. Carlsson, R. Mattsson, P. Gren, M. Elfsberg, and J. Tegnér, “Combination of Schlieren and pulsed TV holography in the study of a high-speed flame jet,” Submitted to Optical Engineering 2004

[10] S. Schedin and P. Gren, “Phase evaluation and speckle averaging in pulsed television holography,” Appl. Opt., 36 (17), pp. 3941-3947, 1997.

[11] G. Pedrini, H. J. Tiziani and Y. Zou, “Digital double pulse-TV-holography,” Opt. Laser Eng., 26, pp. 199-219, 1997.

[12] P. Gren, S. Schedin and L. Xide, ”Tomographic reconstruction of transient acoustic fields recorded by pulsed TV holography,” Appl. Opt., 37 (5), pp. 834–840, 1998.

[13] M. Takeda, H. Ina and S. Kobayashi, “Fourier-transform method of fringe-pattern analysis for computer-based topography and interferometry,” J. Opt. Soc. Am., 72 (1), pp. 156-160, 1982.

[14] L.A. Vasilev, Schlieren methods, Jerusalem, Israel Program, distributed by Keter Inc., New York, 1971.

[15] G.S. Settles, Schlieren and shadowgraph techniques, Springer-Verlag Berlin-Heidelberg New York, 2001.

[16] C. M. Vest, Holographic Interferometry, John Wiley & Sons, New York, 1979.

[17] T. Kreis, Holographic Interferometry, AkademieVerlag GmbH, Berlin, 1996.

[18] O. Marklund, “Interferometric measurements and analysis with applications in elastohydrodynamic experiments,” Doctoral thesis, Luleå University of Technology,1998:29.

[19] N.H. Abel, “Auflosung einer mechanischen Aufgabe,” J. Reine Angew. Math., 1, pp. 153-157, 1826.

[20] C.J. Dasch, “One-dimensional tomography: a comparison of Abel, onion-peeling, and filtered backprojection methods,” Appl. Opt., 31 (8), pp.1146-1152, 1992.

[21] Savitzky and J. Golay, “Smoothing and Differention of data by Simplified Least Squares Procedure,” Analytic Chemistry, Vol. 26, p. 1627, 1964.

[22] W. H. Press, S. A. Teukolsky, W. T. Vetterling and B. P. Flannery, Numerical Recipes in C, Cambridge University Press, Cambridge, pp.650-655, 1992.